Solar Energy Materials & Solar Cells 159 (2017) 20–25

Contents lists available at ScienceDirect

Solar Energy Materials & Solar Cells

journal homepage: www.elsevier.com/locate/solmat

Schottky-type edge passivation of silicon solar cells

Jaeho Choi, Bhaskar Parida, Srikanta Palei, Keunjoo Kim *

Department of Mechanical Engineering and Research Center of Industrial Technology, Chonbuk National University, Jeonju 561-756, Republic of Korea

ARTICLE INFO

Article history:
Received 31 March 2016
Received in revised form
26 August 2016
Accepted 29 August 2016
Available online 8 September 2016

Keywords:
Si solar cell
Edge passivation
Ag nanodots
Schottky barrier

ABSTRACT

We investigated Schottky-type edge passivation of Si solar cells using Ag nanodots and the enhancement of cell conversion efficiency by improving the fill factor. The threshold voltage for the termination of photocurrent is increased by about 0.13 V compared to the reference sample without edge passivation. The cross-section of the pn junction depletion region forms an Ag/Si Schottky contact in the depletion layer of the space and the image charges with a width of about 28 nm. However, the p- and n-electrodes form Ohmic contacts with a contact depletion width of less than 5 nm for the carrier tunneling process. The edge Schottky contact reduces the carrier recombination and saturation current at the surrounding edge region and enhances the fill factor and the pn junction property with increased shunt resistance, indicating that metallic edge passivation is an important process for large-scale Si solar cell fabrication.

1. Introduction

Silicon solar cells have been extensively investigated to improve their conversion efficiency by introducing various surface passivation methods. Surface passivation is involved for the front surface, rear surface, and edge pn junction layers. For the front surface, the light anti-reflection coating (ARC) layer of SiO_x or SiN_x thin films also plays a role in surface passivation. Further, cell passivation has been carried out for thin films such as Al_2O_x and indium tin oxide, hydrogenated a-Si, and low-energy hydrogen ion implantation [1–5]. For the rear contact, a direct contact of Al metal is common for back surface field (BSF) structural formation, along with a local Al contact on the SiO_x layer for the mirror phase structure. For edge passivation, the laser isolation technique is common for pn junction separation. Several authors have reported edge passivation by hydrogen plasma implantation and anodic alumina passivation [6,7]. It remains an important matter for cell edge passivation to prevent carrier leakage.

During the furnace diffusion process, the wafer edge is doped by phosphorus dopant, which can be n-type on the surrounding wafer surface. After cell fabrication, the front and back electrodes can be directly channeled through the pn junction by the edge-isolation process of a laser cut. The edge pn junction cutting process can disconnect the n-type channel on the surrounding front and back surfaces. For more advanced cell fabrication, an additional etching process can remove the n-type layer on the back side, which also removes the n-type layer at the edge side. Then, a SiN_x layer, such as the ARC layer, can form on the front cell area and the edge side by plasma deposition. The pn junction contact with the SiN_x layers provides interfacial defect centers where electron-hole charge recombination happens.

In this work, we investigated the Schottky-type edge passivation effect on Si solar cells by coating the edges of Si solar cells with Ag nanodots. Metal contact on the cell edge did not show a short state or shunt effect, and it increased the conversion efficiency. Photoluminescence and electroluminescence showed reduced spectral emissions at the cell edges. This implies that the metal-semiconductor Schottky contact forms an interfacial barrier to deplete the carriers at the interface.

2. Experimental methods

We used 6in. p-Si(100) wafers with a resistivity of 0.3 Ω-cm for the solar cell fabrication process, as shown in Fig. 1. First, we carried out the saw damage removal and wafer cleaning processes. Then we performed a microtexturing process to form micro-pyramidal structures on the wafer surfaces by etching in a KOH-IPA (isopropyl alcohol) solution at 84.5 °C for 25 min. To form the n-type emitter layer, we performed the phosphorus diffusion process in a tube furnace using $POCl_3$ with a sheet resistance (R_{sh}) of 75 Ω/sq and a surface depth of 100 nm above the doping concentration of 5×10^{19} atoms/cm^3. As advanced cell fabrication, we completely removed the n-type doped layers on the back surface and the surrounding edge sides through an etching process with a 0.5% HF solution. We deposited an 80-nm thick SiNx layer by plasma enhanced chemical vapor deposition (PECVD) at 400 °C for 45 s. The busbars and fingerlines as front contacts were formed by

* Corresponding author.
E-mail address: kimk@chonbuk.ac.kr (K. Kim).

http://dx.doi.org/10.1016/j.solmat.2016.08.033
0927-0248/

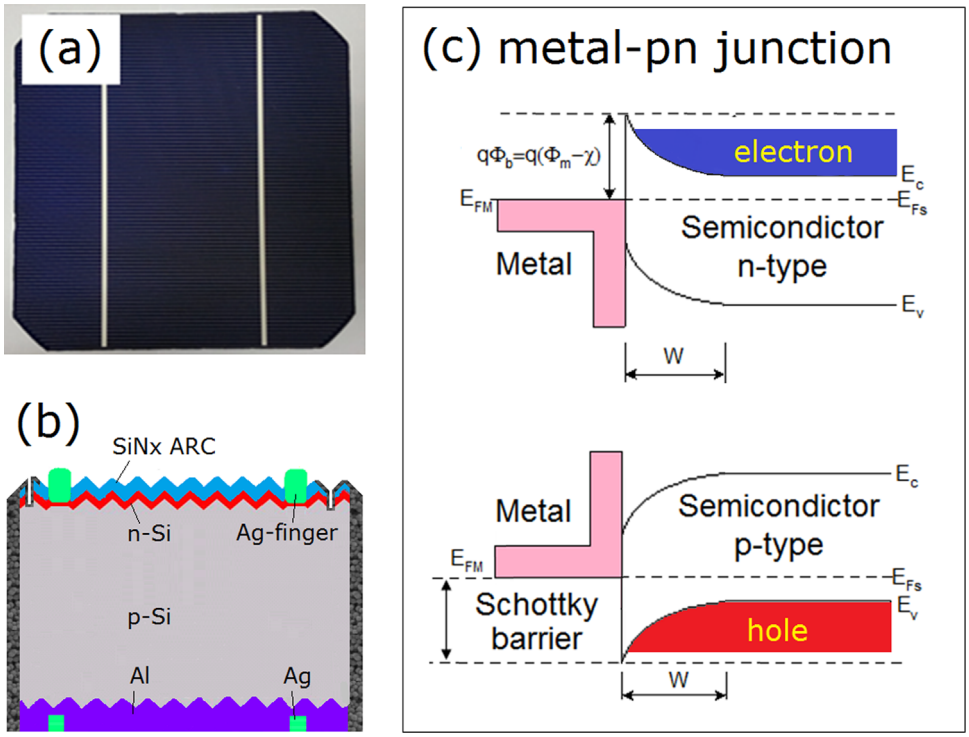

Fig. 1. The fabricated Si solar cell (a) with a schematic diagram (b) of the cross-sectional view with edge passivation by Ag nano-ink and (c) a band diagram of the depletion interface of the Ag-Si Schottky contact with a larger Ag work function (Φ_m) than Si electron affinity (χ). The doped Si surface with stable space charges can contact the Ag metal, and the space charges induce image charges at the metal surface. The space-image charges form a dipole field at the Ag/Si contact, with the depletion width (w) depending on the doping concentration and interfacial potential barrier (Φ_b).

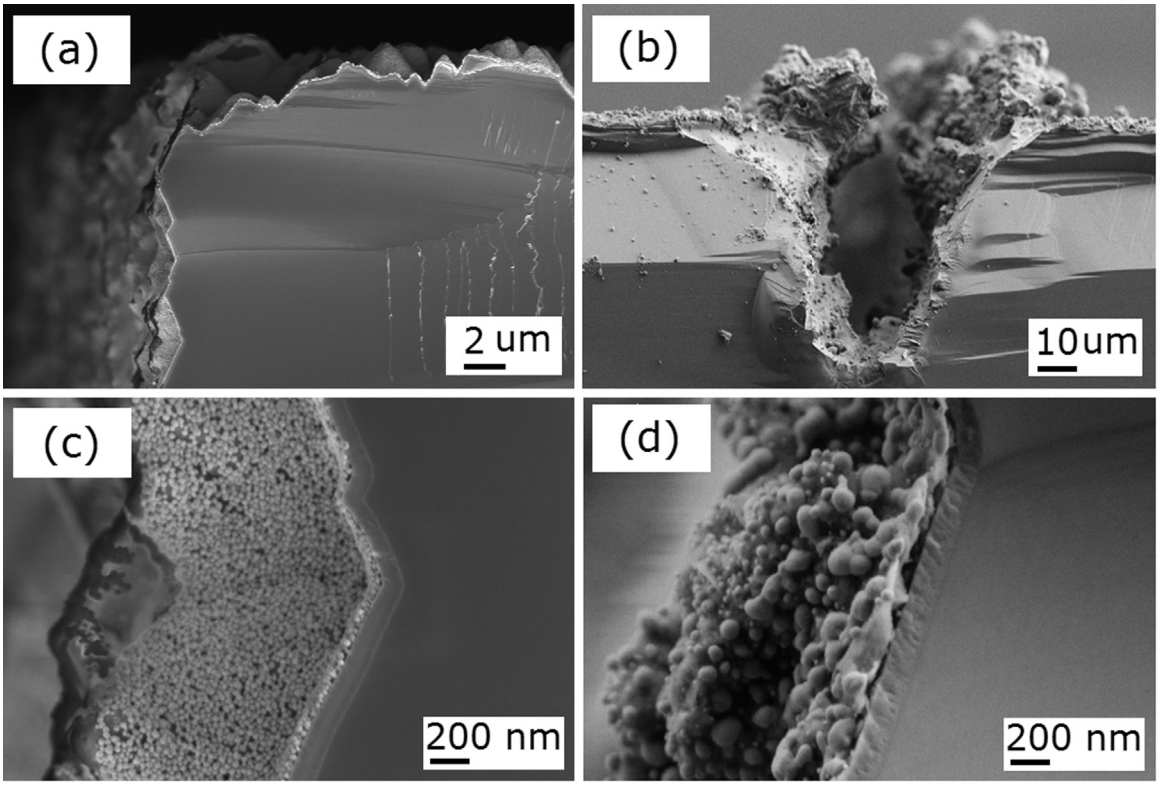

Fig. 2. Cross-sectional FE-SEM images of Si solar cells for edge passivation by Ag nano-ink. The wafer edge was covered by Ag nanodots (a), and the laser-cut region (b) of the edge isolation was also covered with Ag nanodots after the co-firing process. The Ag nanodots are shown in the side region image before (c) and after (d) co-firing, which increases the size of the Ag nanodots.

a screen printing technique using Ag paste, and the back contact was formed using Al paste on the whole area. The laser-cut edge isolation process was performed for all samples. Then, we carried out further edge passivation with Ag nano-ink. We used a brush and roller to coat the edge sides with Ag nanodots. We prepared reference samples (Ref.) with edge sides deposited with a SiNx layer during ARC formation and Ag nanodots-coated samples (Nano Ag) using the Ag nano-ink. Finally, we performed the co-firing process using a belt furnace at process temperatures of 400–870 °C.

We studied the structural, optical, and electrical characteristics of the samples. We characterized the structural properties of the samples using field emission spectroscopy (FE-SEM) and transmission electron spectroscopy (TEM). We studied photoluminescence (PL) and electroluminescence (EL) to analyze the light emission properties from the spectral images of the fabricated cells. Moreover, we studied the quantum efficiency (QE) and current-voltage (I-V) curve to characterize the conversion efficiency of the cells.

3. Results and discussion

The FE-SEM images of the cross-sectional edge surfaces coated with a SiNx ARC layer and Ag nanodots are shown in Fig. 2. The Ag nanodots on the edge of the solar cell were spread over the top of the neighboring surface near the laser-cut region for edge isolation (Fig. 2(a) and (b)). Although Ag nanodots coated the edge sides of the ARC of the solar cells, the Ag nano-ink is water-based and spread onto the front ARC layer, which is hydrophilic. The cross-sectional edge surface was magnified to the side before the co-firing process in Fig. 2(c) and after the process in Fig. 2(d). The size of the Ag nanodots increased after co-firing. The semi-melting Ag nanodots become swollen after the co-firing process and showed penetration into the ARC layer.

Fig. 3 shows cross-sectional TEM images of the interface layer between the Si wafer edge coated by the ARC layer and the Ag nanodots. An interfacial image on the edge of the silicon cell is shown in Fig. 3(a). Si is the lower gray-white region, and platinum (Pt) is the upper dark region. The Pt was deposited on the sample surface to fix the samples. The sharp, dark region that looks like

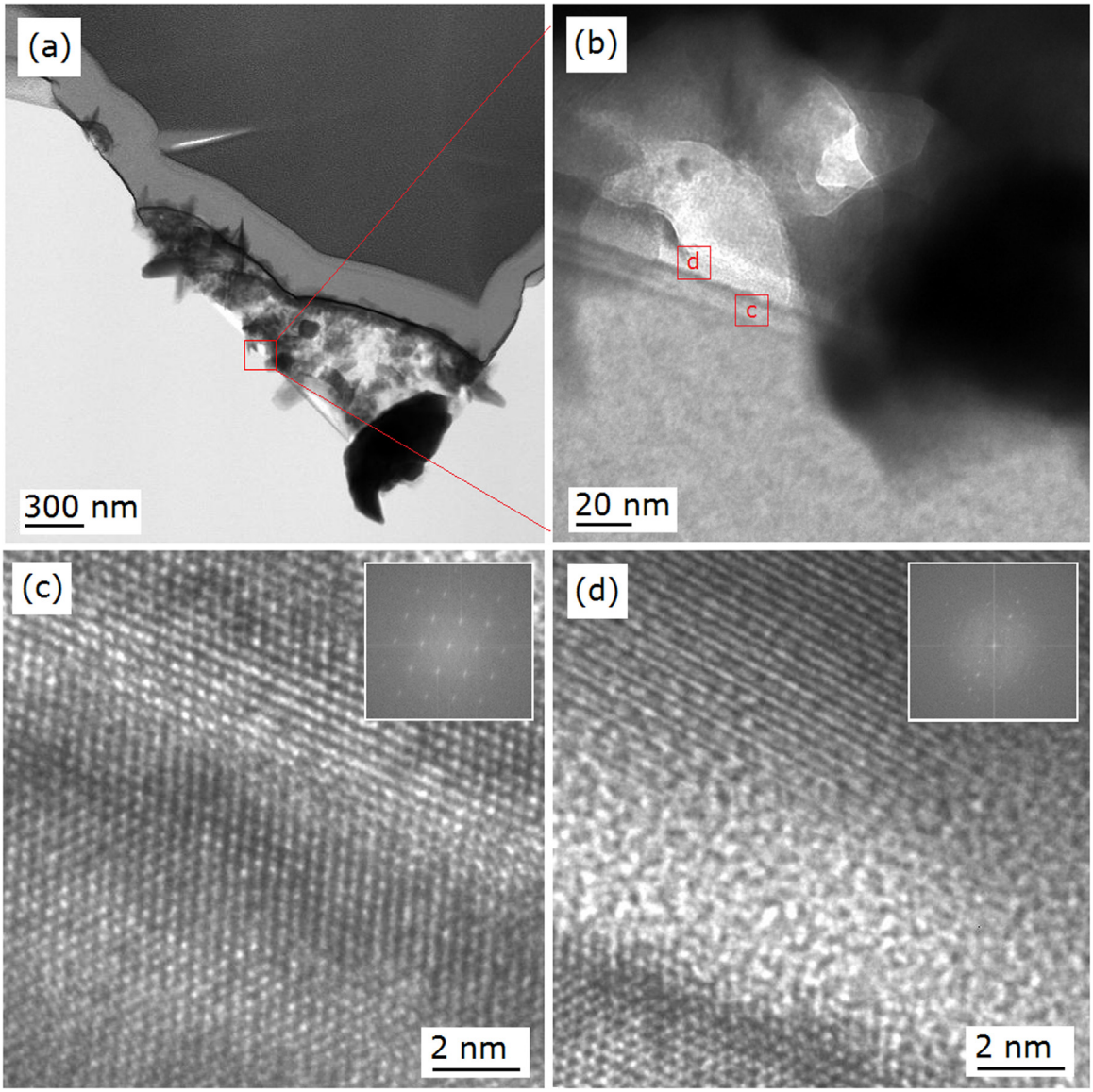

Fig. 3. Cross-sectional TEM images on the side layer of the wafer edge. The Si-SiNx-Ag nanodots interface (b) is rarely shown because after TEM sample preparation, the Ag takes on a dendritic, dark, sharp shape, as shown in (a) and (b) at the interface. The crystalline Si shows a dark contrast with edge residual stress caused by the mechanical cutting process in (c), and the Ag nanodots are diffused onto the amorphous SiNx layer in (d).

trees or leaves consists of Ag dendrites at the Si interface. During the preparation of the TEM samples for measurement, the TEM samples exposed in air showed this dendritic growth of Ag trees outside the Si. The Si interface region is magnified in Fig. 3(b), and the surrounding dark region is the Ag dendrites. The Si surface and amorphous SiNx-Ag alloyed silicate region are further magnified in Fig. 3(c) and (d), respectively. The Si edge surface shows the crystalline phase; the striped layers indicate that the contrast region includes built-in residual stress. However, the electron diffraction image shows a well-oriented crystalline phase. The sandwiched amorphous SiNx layer between the Si surface and the Ag alloyed layer can thus form a Schottky contact at the wafer edge region.

The SEM and TEM images show the formation of an Ag silicate glass layer in the SiNx ARC region, which formed a Schottky contact with the Si surface during the co-firing process. The pn junctions at the edge areas can be the weakest regions in wafers because defect centers, such as residual stress or microcracks, can be involved in the abnormal formation of the depletion regions, and several weak positions of the pn junction can form parallel circuits for the dominant carrier transport process with the smallest shunt resistance [8,9]. This means that carrier separation with a large value of shunt resistance is not possible without considering edge passivation. Generally, Ag paste includes a glass frit to break the amorphous matrix of the SiNx or SiOx layer. However, in nano-ink, Ag nanodots can penetrate the SiOx or SiNx layers without a glass frit. Si cells fabricated with a phosphosilicate glass (PSG) layer above the n-type emitter with a metallic contact via the inclusion of Ag-nanodots printed with nano-ink show enhanced shunt resistance [10]. The printed Ag nanodots can get into the PSG layer and form an Ohmic contact between the n-type Si emitter layer and the metal electrode. The Ag atoms can also easily diffuse into the defect zones, such as microcracks and dislocations with residual stress. The edge passivation can be seen from the change in the intensity of the carrier recombination process.

Fig. 4 shows photographic PL and EL images for the Ref. and Nano Ag samples. Both samples showed high PL spectra, indicating that the pn junction formation is well established during the diffusion process. The PL image of the Ref. sample in Fig. 4(a) shows brightness in all parts, even at the edges, but the upper part of the Nano Ag sample shown in Fig. 4(b) is dark, and the surrounding edge regions are darker than those in the Ref. sample. This means that radiative recombination in those regions is reduced by the Ag edge passivation. A crack in the bottom of the Nano Ag cell is passivated by the Ag nanodots, as shown in the reduced PL image. The Ref. EL image in Fig. 4(c) is very bright except for the center part and does not have uniform spectra, unlike the PL image. However, the images correspond in several mini spots. The EL image for the Nano Ag sample in Fig. 4(d) is less bright than the Ref. sample, and the spectra are well-matched with the corresponding dark spots in the PL image. In both the PL and EL images, the surrounding edges are involved with defects in light emissions. The Nano Ag sample has darker images than the Ref. sample, which means that the brightness can be reduced by edge passivation.

The darkness of both images in the upper parts of the Nano Ag sample indicates non-radiative recombination or a no-flow of holes and electrons through the abnormal formation of the pn junction. However, the straight contrast lines from the dark part of the EL image indicate that the fingerlines could not form a proper Ohmic contact and show a rare current flow caused by high

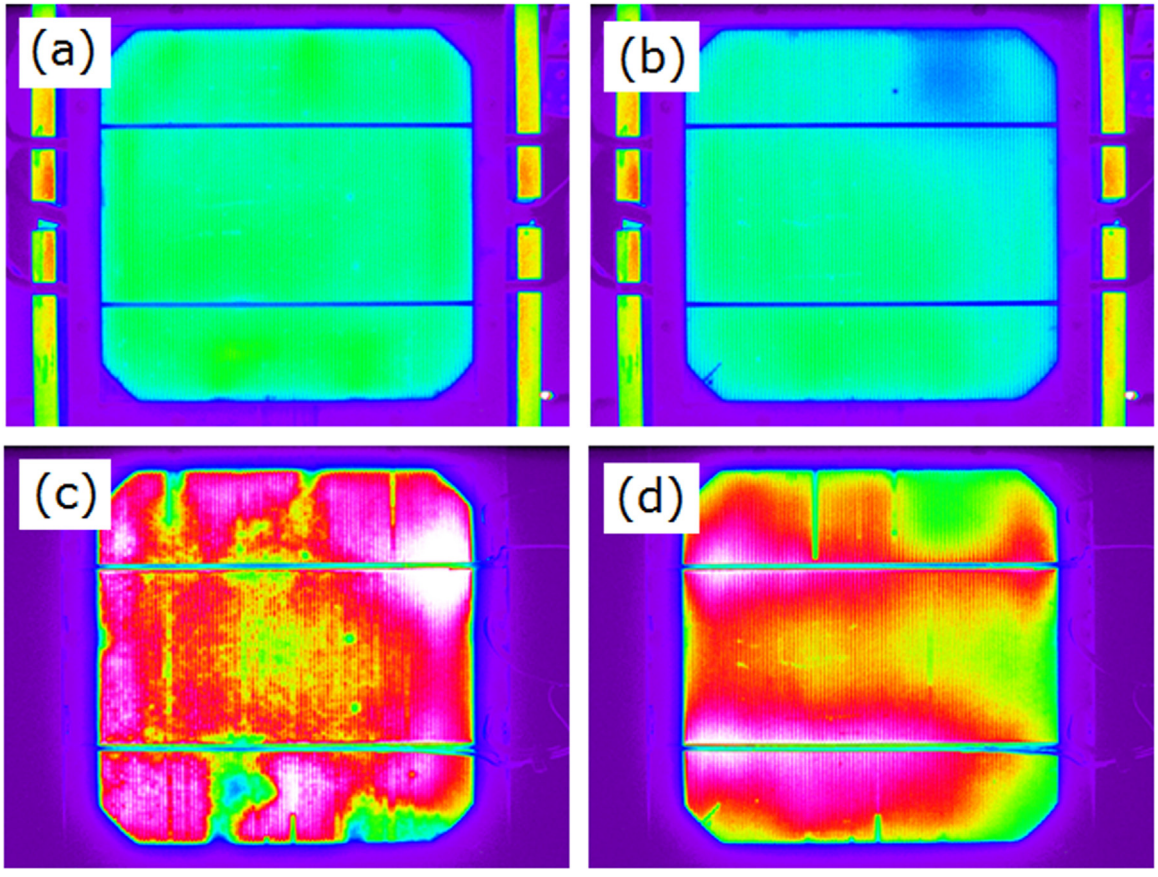

Fig. 4. Photographic images of PL (a, b) and EL (c, d) for the fabricated Si solar cells for the Ref. (a, c) and Nano Ag samples (b, d). The Nano Ag sample showed reduced PL and EL emissions compared with those of the Ref. sample, especially at the edge regions.

resistance. The metal contact to the pn junction can form a Schottky barrier at the interface to deform the band structure, and the electron and hole carriers can be depleted from the Schottky contacts [11–13]. Similarly, when comparing the Nano Ag cell with the Ref. sample, the radiative recombination intensities for both the PL and EL spectra were reduced at the surrounding edge regions, indicating the formation of a Schottky barrier at the pn junction depletion regions, which in turn shows that the various defects at the edge regions can be cured by metallic passivation to prevent edge leakage. We further examined the carrier influence on edge passivation using measurements of internal QE and conversion efficiency.

Fig. 5 shows the QE for the Ref. and Nano Ag samples. The QE of the Ref. sample was about 78% in the spectral range between 500 and 900 nm, whereas the QE of the Nano Ag sample was about 89%. The Ref. sample shows relatively low QE in spite of the high radiative recombination process shown by the bright PL and EL emissions. The Nano Ag sample showed enhanced QE compared with the Ref. sample. In the short wavelength region of 400–600 nm, the Nano Ag sample showed a QE greater than 90%. The QE is the measure of the internal photon-carrier conversion and indicates a ratio of the number of incident photons that can be converted into the number of carriers inside the material. In our samples, edge passivation showed a strong influence on QE. In spite of the big difference in internal QE, the external conversion

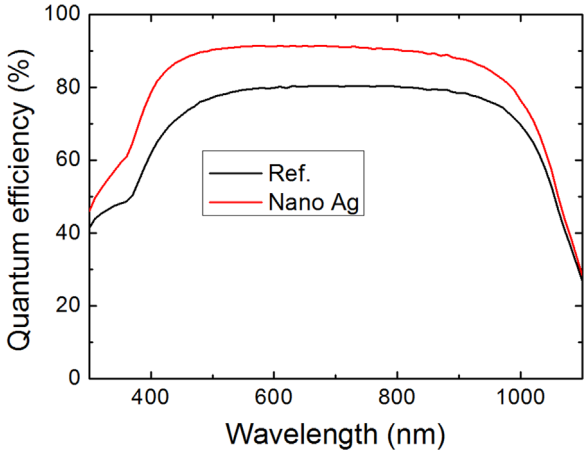

Fig. 5. The quantum efficiencies of the Ref. and Nano Ag Si solar cells.

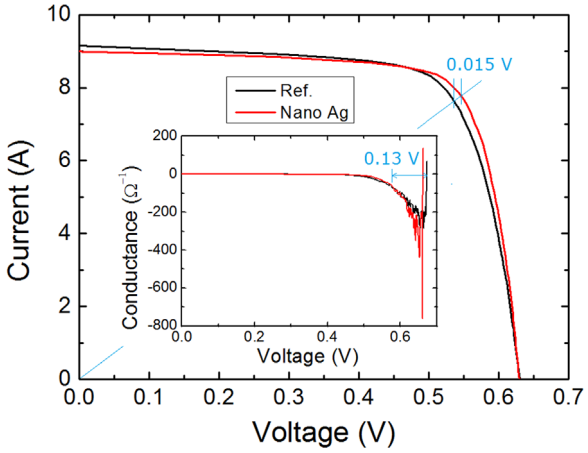

Fig. 6. The current–voltage (I-V) measurement for the Ref. and Nano Ag samples by solar simulator at 1-sun under AM1.5 G irradiation. The inset is the conductance, which fluctuated largely and terminated at the open circuit voltage.

Table 1
Fabricated cell properties of the Ref. samples made using standard cell fabrication and Nano Ag samples made using an additional metal edge-passivation process. The represented values show the median values for conversion efficiency, and dispersion values come from the minimum and maximum values of three fabricated 6 in. Si solar cells.

Sample	Eff. [%]	Voc [V]	Isc [A]	FF [%]	Rs [Ω]	Rsh [Ω]
Ref.	17.52 −0.02/ +0.18	0.630 −0.01/0	9.155 0/+0.022	72.62 −0.09/ +0.68	0.002 −0.001/ +0.001	2.693 −0.083/ +0.126
Nano Ag	18.02 −0.01/ +0.14	0.629 −0.001/0	8.989 −0.005/ +0.033	76.14 0/+0.48	0.002 −0.001/0	2.886 0/+0.811

efficiency showed very similar values, with only a small difference in the I-V measurements.

Fig. 6 shows the I-V curve for the Ref. and Nano Ag cells measured using a solar simulator at 1-sun under AM1.5 G irradiation. The electrical performance data for the cells are listed in Table 1. The Ref. cell had a conversion efficiency of 17.52% with dispersion ranges of −0.02/+0.18% for several measurements, and the Nano Ag edge passivated cell had an efficiency of 18.02% with dispersion ranges of −0.01/+0.14%. The open circuit voltages show similar values between the Ref. and Nano Ag cells. However, for the short circuit current, the Ref. sample showed a larger value than Nano Ag sample. The fill factor value for the Nano Ag passivated cell showed a large enhancement compared with the Ref. sample, achieving a voltage increase of about 0.015 V at the line of maximum power. However, the series and shunt resistances were very similar for the same cell fabrication process. The inset shows the differential current with respect to the voltage, indicating the conductance. When the forward voltage bias was increased to reach the open circuit voltage, the carrier conductance fluctuated strongly, and the photocurrent was terminated. The threshold voltage for carrier tunneling is 0.13 V. The Nano Ag cell shows steeper termination and lower conductance than the Ref. sample.

As shown in Fig. 1, the Schottky barrier heights for the contact between the Ag metal and crystalline Si depend on the doping levels and the crystalline directions on the adatom surface structure of the Ag [14–16]. The emitter surface with a surface doping level above $5 \times 10^{19}/cm^3$ provided a Ag/Si contact depletion layer of about w=2.8 nm, indicating Ohmic contact by carrier tunneling via the field emission mechanism. For the back contact with Al, the Al/Si contact formed an Al-doped BSF layer for the Ohmic contact. However, the edge Ag/Si contact with a cross-sectional n-type emitter layer was involved with various doping levels. In the pn junction region below a doping level of $5 \times 10^{17}/cm^3$, the Ag/Si contact formed a depletion width of w=28 nm. The heavily doped surface region formed an Ohmic contact, and the decreased doping level near the pn junction formed a Schottky contact with an increased depletion layer. For a low p-type doping cross-section, a wide depletion layer also provided the formation of a Schottky contact by the thermionic emission mechanism.

The Ag atoms formed an adsorption geometry of $(\sqrt{3} \times \sqrt{3})$ Ag on a Si(111) (7×7) surface and a non-ideal hexagonal honeycomb Ag structure on a microtextured Si solar cell [16]. For the heavily doped n-type case, The barrier height of the emitter contact on the microtextured Si(111) surface was 0.75 eV, and the wafer edge barrier on the Si(100) surface was 0.72 eV. The barrier difference is thus about 0.03 eV. For the heavily doped p-type, the BSF layer on the microtextured Si(111) surface was formed by the Al back contact and had a barrier of 0.48 eV, whereas the wafer edge on the lightly doped p-type Si(100) surface with a Ag metal contact had a barrier of 0.35 eV [14,17], for a barrier difference of about

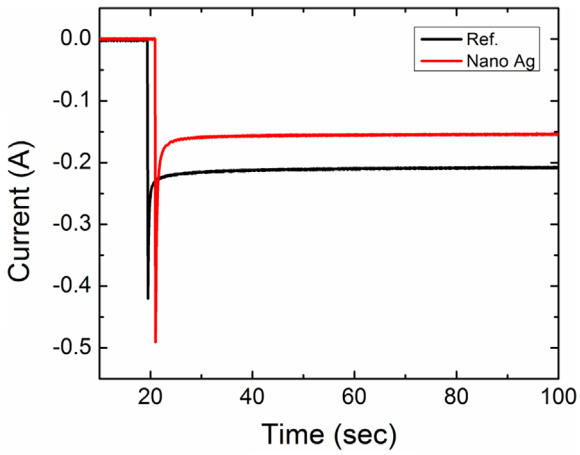

Fig. 7. The dark state saturation currents of the Ref. and Nano Ag cells as a function of time and a constant external reverse bias of −1.5 V.

−0.12 eV. Therefore, for n-type layers, the Ag metal edge barrier height was slightly smaller than for the n-emitter contact barrier, and for p-type layers, the back Al barrier was somewhat larger than the edge Ag barrier. Therefore, the main Ag/Si contact factor comes from the contact depletion width rather than the barrier height for Schottky contact formation. Edge passivation by Ag nanodots does not cause the pn junction shunt effect but enhances the fill factor by forming a metal-semiconductor Schottky barrier, which prevents leakage current from mechanically induced edge defects.

Fig. 7 shows the dark state saturation currents (I_0) of the Ref. and edge passivated Si solar cells. The saturation currents were measured by a Labpro Vernier system with an external reverse bias of −1.5 V. It can be clearly seen that when the reverse bias of −1.5 V is applied, currents are increased rapidly in the first several seconds and saturated at certain values. The I_0 values of the Ref. and Nano Ag cells are −0.21 (−0.863) and −0.15 A (−0.616 mA/cm^2), respectively. This result reveals that the nano Ag cell shows a lower I_0 than the Ref. cell, which indicates that the leakage current and the carrier recombination at the edge of the cell is reduced by the Nano Ag passivation.

It is considered that I_0 is a key parameter of the recombination center in equilibrium, i.e. large recombination centers generate high saturation current [18,19]. The diffusion current is strongly related to the series resistance and the open circuit voltage under the forward bias with the factor n=1. The trap concentration of the defect centers is related to the recombination current with the factor n=2 [19]. The reverse saturation current is correlated with the recombination current. The edge passivation provides no change in the open circuit voltage and series resistance, but improves the reverse saturation current with the enhanced fill factor. Therefore, the Nano Ag is effective in passivating the edges of the Si solar cells and minimizing the saturation current related to the defect centers at the edges to enhance the conversion efficiency.

4. Conclusions

We investigated edge passivation on the exposed pn junction for 6 in. Si solar cells using a coating of Ag nanodots as a cell fabrication process. The edge Schottky contacts strongly reduce radiative recombination at the surrounding wafer edges, as seen from the PL and EL emissions. Edge passivation also enhances the quantum efficiency of the cells, which becomes an increase in conversion efficiency. The enhanced conversion efficiency is related to the cell property of an improved fill factor. Metallic edge passivation did not decrease the cell property by the shunting phenomenon, but instead formed a Schottky contact at the cross-sectional pn junction depletion region with a large contact depletion width, indicating enhanced conversion efficiency by an increased threshold voltage for defect saturation at the surrounding wafer edge regions. Metallic edge passivation is thus crucial as an elemental process in the standard fabrication of large-scale Si solar cells.

Acknowledgments

This research was supported by the Basic Science Research Program through the National Research Foundation of Korea (NRF) funded by the Ministry of Education under Grant (NRF-2014R1A1A2056184). This paper was also supported by research funds of Chonbuk National University in 2015 (CBNU-2015).

References

[1] P.J. Zanzucchi, C.R. Wronski, D.E. Carlson, Optical and photoconductive properties of discharge-produced amorphous silicon, J. Appl. Phys. 48 (1977) 5227–5236.
[2] A. Wang, J. Zhao, M.A. Green, 24% efficient silicon solar cells, Appl. Phys. Lett. 57 (1990) 602–604.
[3] J. Li, J., M. Chong, J. Zhu, Y. Li, J. Xu, P. Wang, Z. Shang, Z. Yang, R. Zhu, X. Cao, 35% efficient nonconcentrating novel silicon solar cell, Appl. Phys. Lett. 60 (1992) 2240–2242.
[4] G. Guttler, H.J. Queisser, Impurity photovoltaic effect in silicon, Energy Convers. 10 (1970) 51–55.
[5] T. Zundel, A. Mesli, J.C. Muller, P. Siffert, Boron neutralization and hydrogen diffusion in silicon subjected to low-energy hydrogen implantation, Appl. Phys. A 48 (1989) 31–40.
[6] A. Rohatgi, D.L. Meier, P. Rai-Choudhury, S.J. Fonash, R. Singh, Effect of low-energy hydrogen ion implantation on dendritic web silicon solar cells, J. Appl. Phys. 59 (1986) 4167–4171.
[7] J.C. Muller, A. Barhdadi, Y. Ababou, P. Siffert, Hydrogen ion passivation of multicrystalline silicon solar cells, Rev. Phys. Appl. 22 (1987) 649–654.
[8] G. Guo, W. Gan, F. Xiang, J. Zhang, H. Zhou, H. Liu, J. Luo, Effect of dispersibility of Silver powders in conductive paste on microstructure of screen-printed front contacts and electrical performance of crystalline silicon solar cells, J. Mater. Sci. Mater. Electron. 22 (2011) 527–530.
[9] H. Yang, X. Lei, H. Wang, M. Wang, Investigation of contact resistance between silicon and silver paste made by screen-printing, Clean Technol. Environ. Policy 15 (2013) 1049–1053.
[10] J. Choi, B. Parida, H.Y. Ji, S. Park, K. Kim, Ohmic contact effect of Ag-nanodots on quantum efficiency of Si solar cell, J. Nanosci. Nanotechnol. 12 (2012) 5552–5557.
[11] V.P. Popov, I.E. Tyschenko, L.N. Safronov, O.V. Naumova, I.V. Antonova, A. K. Gutakovsky, A.B. Talochkin, Properties of silicon oversaturated with implanted hydrogen, Thin Solid Films 403–404 (2002) 500–504.
[12] D.C. Leung, P.R. Nelson, O.M. Stafsudd, J.B. Parkinson, G.E. Davis, Efficient lateral minority carrier transport in proton-implanted p-type silicon, Appl. Phys. Lett. 67 (1995) 88–90.
[13] M. Ichimura, H. Sakakibara, K. Wada, M. Kato, Efficiency of a solar cell with intermediate energy levels: an example study on hydrogen implanted Si solar cells, J. Appl. Phys. 114 (2013) 114505–114506.
[14] H.H. Weitering, J.P. Sullivan, R.J. Carolissen, R. Pérez-Sandoz, W.R. Graham, R. T. Tung, Inhomogeneous Schottky barriers at Ag/Si(111) and Ag/Si(100) interfaces, J. Appl. Phys. 79 (1996) 7820–7829.
[15] Y.G. Ding, C.T. Chan, K.M. Ho, Structure of the ($\sqrt{3}\times\sqrt{3}$) R 30° Ag/Si(111) surface from first-principles calculations, Phys. Rev. Lett. 67 (1991) 1454–1457.
[16] S. Kono, T. Abukawa, N. Nakamura, K. Anno, Reinvestigation of the structure of Si(111) $\sqrt{3}\times\sqrt{3}$-Ag surface, Jpn. J. Appl. Phys. 28 (1989) L1278–L1281.
[17] Zs.J. Horvath, M. Adam, I. Szabo, M. Serenyi, Vo. Van Tuyen, Modification of Al/Si interface and Schottky barrier height with chemical treatment, Appl. Surf. Sci. 190 (2002) 441–444.
[18] A. Cuevas, The recombination parameter J_0, Energy Procedia 55 (2014) 53–62.
[19] K. Kurobe, H. Matsumani, New two-diode model for detailed analysis of multicrystalline silicon solar cells, Jpn. J. Appl. Phys. 44 (2005) 8314–8321.